IR Kinetic Spectroscopy Investigation of the $CH_4 + O(^1D)$ Reaction

Hong-bing Chen, W. D. Thweatt, Jinjin Wang, Graham P. Glass,* and R. F. Curl*

Chemistry Department and Rice Quantum Institute, Rice University, Houston, Texas 77005

Received: October 1, 2004; In Final Form: January 10, 2005

The branching of the title reaction into several product channels has been investigated quantitatively by laser infrared kinetic spectroscopy for CH_4 and CD_4. It is found that OH (OD) is produced in 67 ± 5% (60 ± 5%) yield compared to the initial $O(^1D)$ concentration. H (D) product is produced in 30 ± 10%(35 ± 10%). H_2CO is produced in 5% yield in the CH_4 system (it was not possible to measure the CD_2O yield in the CD_4 case). D_2O is produced in 8% yield in the CD_4 system (it was not feasible to measure the H_2O yield). The ratio of the overall rate constant of the CD_4 reaction to the overall rate constant of the $O(^1D) + N_2O$ reaction was determined to be $1.2_5 \pm 0.1$. A measurement of the reaction of $O(^1D)$ with NO_2 gave 1.3×10^{-10} cm^3 molecule^{-1} s^{-1} relative to the literature values for the rate constants of $O(^1D)$ with H_2 and CH_4. Hot atom effects in $O(^1D)$ reactions were observed.

Introduction

Methane is the most abundant hydrocarbon in the atmosphere and consequently one of the most important atmospheric species. The reaction of methane with $O(^1D)$ is a source for stratospheric OH, and that oxidation is also a source of a portion of stratospheric H_2O, which itself is a source of OH through reaction with $O(^1D)$. These reactions occur in the region of high ozone concentration at altitudes from about 20 to 50 km, where hydroxyl radical (OH) can cause the catalytic destruction of very large quantities of ozone via the HO_x cycles.[1,2]

Since the reaction of $O(^1D)$ with CH_4 is important in the atmosphere, it has been studied many times previously using various experimental and theoretical methods. The reaction is extremely fast: most reported[3−5] rate constants cluster around 1.5×10^{-10} cm^3 molecule^{-1} s^{-1} except for one measurement[6] of 3.8×10^{-10} cm^3 molecule^{-1} s^{-1} and another[7] of $2.2 \pm 0.2 \times 10^{-10}$ cm^3 molecule^{-1} s^{-1}. The JPL compilation[8] recommends a value of the total reaction rate constant of 1.5×10^{-10} cm^3 molecule^{-1} s^{-1}.

The reaction has numerous exothermic channels, some of which are listed below:

$$O(^1D) + CH_4 \rightarrow CH_3 + OH \qquad \Delta H = -179 \text{ kJ/mol} \quad (1a)$$

$$\rightarrow CH_2OH + H \qquad \Delta H = -172 \text{ kJ/mol} \quad (1b)$$

$$\rightarrow CH_3O + H \qquad \Delta H = -128 \text{ kJ/mol} \quad (1c)$$

$$\rightarrow H_2CO + H_2 \qquad \Delta H = -473 \text{ kJ/mol} \quad (1d)$$

$$\rightarrow H_2CO + 2H \qquad \Delta H = -37 \text{ kJ/mol} \quad (1e)$$

$$\rightarrow {}^1CH_2 + H_2O \qquad \Delta H = -176 \text{ kJ/mol} \quad (1f)$$

$$\rightarrow O(^3P) + CH_4 \qquad \Delta H = -439 \text{ kJ/mol} \quad (1g)$$

Here, the reaction enthalpies were calculated using data from Atkinson et al.[9]

The branching ratios for the major channels have been measured by a number of groups, and it is now well established that the dominant products of $O(^1D) + CH_4$ are $CH_3 + OH$. Lin and DeMore[10] analyzed the final products of photolyzed mixtures of N_2O/CH_4 and concluded that (1a) accounted for 90% and (1d) accounted for 9% of the observed products. Addison et al.[11] reported an OH yield of 80%. Casavecchia et al.[12] used a molecular beam apparatus to observe H and CH_2-OH (or CH_3O) products, and reported that the yield of H_2 was <25% of the yield of H. Satyapal et al.[13] observed H atoms in a pulsed laser experiment and reported a yield of H of (25 ± 8)%. Matsumi et al.[7] measured the yields of H and $O(^3P)$ in low-pressure gas mixtures as (15 ± 3)% and <5% respectively. Wine and Ravishankara[14] reported that the yield of $O(^3P)$ was <4.3%, and Takahashi et al.[15] reported that it was <1%. In 1998, the branching ratio for the H formation channel was measured by Brownsword et al.[16] at somewhat higher collision energies as 30 ± 11%. In 1999, Lin et al.[17] reported the amount of H_2 produced as only 30% of the amount of H produced and suggested that the main channel producing atomic H was CH_2-OH (hydroxymethyl) + H with the CH_3O(methoxy) + H channel at most a minor contributor. In 1995, Hack and Thiesemann[18] determined the following product ratios: $\Phi(CH_2O) = 0.06 \pm 0.01$, $\Phi(CH_2(\tilde{a})) = 0.02 \pm 0.01$, and $\Phi(O(^3P)) = 0.02 \pm 0.01$. The recent JPL recommended branching ratios are (a) 75% ± 15%, (b) 20 ± 7%, and (c) 5 ± 5%, with great uncertainties.[8]

Because this reaction system is small enough to be attacked by theoretical calculations, accurate experimental branching ratios will be of value for comparisons with such calculations.

In the present investigation, the reaction of $O(^1D)$ with methane was studied by using infrared kinetic spectroscopy to measure the yields of the channels producing OH, CH_3, H, H_2CO, CH_3O, and $H_2O(D_2O)$ at thermal energies. The rate constant of the title reaction was also remeasured relative to $O(^1D) + N_2O$ reaction.

Experimental Section

The technique of infrared kinetic spectroscopy was employed for this work. All experiments were carried out in a large excess of helium, which served as a buffer gas, and at total pressures of 12∼70 Torr. Since hot atom effects were observed in the

* To whom correspondence should be addressed.

10.1021/jp045521d CCC: $30.25
Published on Web 02/22/2005

low-pressure regime for $O(^1D)$ reactions, all measurements to quantify the reaction channels under thermalized conditions were carried out at ~66 Torr. $O(^1D)$ was generated by flash photolysis of N_2O and NO_2 ($[O(^1D)]_0 \approx 5 \times 10^{12}$cm^{-3}; see below) using an ArF laser at 193 nm. CH_3 and OH are known to be the main products of the $O(^1D) + CH_4$ reaction. There are large discrepancies in the literature rate constant measurements for the reaction between CH_3 and OH, but a rate constant of about 10^{-10} cm^3 molecules^{-1} s^{-1} is slightly larger than the highest rates reported. Using this value for the rate constant, the 1/e time calculated for $CH_3 + OH$ assuming all $O(^1D)$ is converted to these species is 2 ms. Thus observations made in the first 100 μs should not be affected by radical−radical chemistry.

Under all of our conditions, vibrationally excited CH_3 is effectively relaxed by He with $\tau = 8$ μs at ~12 Torr He. However, vibrationally excited OH is not quickly relaxed in the photolysis system using N_2O. Therefore, in this system about 8~25% NO was added to the N_2O in order to relax OH within 20 μs. As is always the case in this kind of experiment, care had to be taken to avoid contaminating the chemistry through product build-up or reagent depletion by keeping the flash repetition rate low and the total gas flow rate high. Apart from these concerns, the essential experimental concerns for these experiments are the measurement of infrared absorption and the measurement of reagent concentrations. These are described below.

Infrared Kinetic Spectroscopy Apparatus and Intensity Measurements. The experimental apparatus is the same as that used previously[19] for the investigation of the reaction between OH and CH_3CHO. Only a brief description of the experimental conditions is given here. In these experiments, mixtures containing $O(^1D)$ source N_2O (or NO_2), reagents (H_2, CH_4, CD_4, etc.), and excess helium buffer gas were photolyzed at 193 nm, by using an ArF excimer laser. The 2 m (actually 1.83 m) Herriott cell is based upon the modification of the standard design described by Pilgrim and co-workers.[20] The cell was operated at 31 passes. The probe laser beam only overlaps the photolyzed region in the central portion of the cell giving a total usable path length of ~20 m (~0.64 × 31). All infrared frequencies employed were generated by difference frequency mixing of a Coherent Autoscan Ti:sapphire laser with a single frequency Nd:YAG in periodically poled $LiNbO_3$ (PPLN). The line width (about 1 MHz) of the resulting infrared probe was much narrower than the line widths (typically 200 MHz) of the individual rovibrational transitions monitored.

To carry out quantitative measurement of the infrared absorbances, the probe IR frequency was scanned over the line in 20 MHz steps. At each frequency step, the excimer photolysis laser was fired about 10 times, and the entire time profile relevant to the experiment was acquired with a transient digitizer. Time-correlated noise was then removed from the data thus acquired by subtracting the time channel immediately before the excimer firing from the rest of the channels. This substantially denoised data was then analyzed by fitting a Gaussian line shape to the data at each time. Four parameters were fitted: peak height, line width, center frequency, and baseline. In some situations, the line width parameter was known and could be fixed thereby reducing the fit parameters to three; in some cases the central frequency was also known thereby reducing the fit parameters to two.

This method for acquiring and treating data has the advantage that if pressure broadening ever becomes significant, the data can be fitted with a Voigt profile and integrated intensities calculated. The fitting process is organized so that the quality of the fit at any time point can be examined. In typical practice, a number of time points shortly after the flash when the signal is largest are examined. Based upon examinations of these fittings, the center frequency and line width can be fixed and the two parameter fitting is then allowed to proceed automatically into the longer time region where the data is often much noisier. These multiple least-squares fittings also provide the estimated standard deviations of the parameters at each time allowing error bars for the peak heights to be obtained.

Reagents and Concentration Measurements. The reaction studied here is extremely fast ($k > 10^{-10}$ cm^3 s^{-1}). This means that there is little concern that a minor impurity will consume a significant portion of the radical pool. As radical products tend to react rapidly, secondary reactions can be, and on some occasions are, important, but again minor impurities have little impact. Because the helium buffer gas is present at a much higher concentration than any other reagents, an impurity in the helium conceivably might be a problem. However, the helium used was of very high purity (99.999%). Standard commercial chemicals were used in this work for all other reagents, and no special effort was made to purify them.

Flow controllers were used to set the flow of gaseous reagents (He, CH_4, N_2O, H_2, D_2, and CD_4). For NO_2, the pressure drop in a known volume in known time taking into account the equilibrium $2NO_2 \leftrightarrow N_2O_4$ was used to calculate the flow rate. Careful calibrations were made for various gaseous reagents and flow meters. The reagent concentrations are then calculated from the equation

$$C_j = \frac{F_j}{\sum_i F_i} \frac{gN_0}{RT} \frac{P_{tot}}{760} \qquad \text{(I)}$$

where C_j is the concentration of species j (molecules/cm^3), F_j is the flow rate of species j (sccm), N_0 is Avogadro's number, R is the gas constant (cm^{3}atm/(mol K), and P_{tot} is the total pressure (Torr).

In this study, two different sources of $O(^1D)$ were used, the 193 nm photolysis of N_2O and the 193 nm photolysis of NO_2

$$N_2O + h\nu\ (193\ \text{nm}) \rightarrow O(^1D)(100\%) + N_2 \qquad (2)$$

$$NO_2 + h\nu\ (193\ \text{nm}) \rightarrow O(^1D)(55\%) + NO \qquad (3)$$

N_2O has an absorption cross section of 9×10^{-20} cm^2 at 193 nm [21] and a quantum yield for $O(^1D)$ of 1.[22] The absorption cross-section of NO_2 at 193 nm is approximately 3×10^{-19} cm^2, and the quantum yield of $O(^1D)$ is 0.55.[23]

N_2O is relatively inert, suppressing secondary chemistry. Its concentration can be easily and reliably measured and does not change during the experiment; furthermore, the reaction of $O(^1D)$ with N_2O produces only a small amount of $O(^3P)$ producing instead 2NO or $N_2 + O_2$. Unfortunately, the partial pressure of N_2O in the system had to be kept large (about 250 mTorr) because of its small cross-section. N_2O removes $O(^1D)$ rapidly from the system by the reaction

$$O(^1D) + N_2O \rightarrow 2NO \qquad k_{4a} = 6.7 \times 10^{-11}\ \text{cm}^3\ \text{s}^{-1} \qquad (4a)$$

$$\rightarrow N_2 + O_2 \qquad k_{4b} = 4.8 \times 10^{-11}\ \text{cm}^3\ \text{s}^{-1} \qquad (4b)$$

with a total rate constant[8] $k_4 = 1.16 \times 10^{-10}$ cm^3 molecule^{-1} s^{-1} and thus competes with CH_4 for $O(^1D)$.

NO_2 was used primarily for the purpose of searching for H atom products by converting H to OH through the reaction

$$H + NO_2 \rightarrow OH + NO \qquad k_5 = 1.3 \times 10^{-10}\ cm^3\ s^{-1} \quad (5)$$

In contrast with N_2O, NO_2 is highly reactive creating a rich secondary chemistry.

3. Observations and Results

(a) Hot Atom Effects. To test our methodology, we decided to measure the rate constant of the reaction

$$O(^1D) + H_2 \rightarrow OH + H \qquad k_6 = 1.1 \times 10^{-10}\ cm^3\ s^{-1} \quad (6)$$

relative to that of $O(^1D) + N_2O$ (reaction) assuming that reaction 6 has only the channel shown.[8] The expected peak OH absorbance (base e) (extrapolated back to the time of the flash) upon photolysis of a mixture of H_2 and N_2O with a small amount of NO added to relax vibrationally excited OH (this has been discussed previously) can be expressed as

$$A(OH) = \sigma L \frac{k_6[H_2]}{k_6[H_2] + k_4[N_2O] + k_7[NO]}[O(^1D)]_0 \quad (II)$$

where σ is the OH absorption cross-section, L is the path length of the probe laser where the probe overlaps the photolyzed region, and the other quantities are rate constants and concentrations. $[O(^1D)]_0$ is the initial $O(^1D)$ concentration. Here, k_7 is the rate constant of the reaction

$$O(^1D) + NO \rightarrow \text{products} \qquad k_7 = 0.6 \times 10^{-10}\ cm^3\ s^{-1} \quad (7)$$

This estimate for the rate constant for (7) is from our observations in the changes of the slopes of Stern−Volmer plots as [NO] is varied; we could find no recent measurements of this reaction rate constant. The expression above can be rearranged to

$$\frac{1}{A(OH)} = \frac{1}{\sigma L[O(^1D)]_0}\left(1 + \frac{k_4[N_2O] + k_7[NO]}{k_6}[H_2]^{-1}\right) \quad (III)$$

Thus, if $1/A(OH)$ is plotted vs $1/[H_2]$, a straight line is expected with the ratio of the slope to intercept being $(k_4[N_2O] + k_7[NO])/k_6$. Figure 1a shows such a Stern−Volmer plot in a system where the partial pressure of N_2O is 362.8 mTorr and the partial pressure of the helium buffer gas is 12 Torr. The solid line on this graph is the best fit to the data adjusting only the quantity $\sigma L[O(^1D)]_0$ with k_6 and k_4 fixed to the literature values of 1.1×10^{-10} and 1.16×10^{-10} cm^3 $molecule^{-1}$ s^{-1}, respectively, and $k_7 = 6 \times 10^{-11}$ cm^3 $molecule^{-1}$ s^{-1}. The ratio of the slope to the intercept for the best linear fit (dotted line in Figure 1a) is a factor of 1.8 smaller than the same ratio as predicted from the accepted rate constants.

This major disagreement cannot be caused by reagent depletion or product build-up. At 1000 sccm He flow rate, the volume flow rate at 10 Torr is about 1400 cm^3/s. The cell volume from the point where the N_2O is introduced to the end of the observation zone is about 14 L. Thus, it takes approximately 10 s from the beginning of exposure of N_2O to exit from the observation zone. Each laser pulse contains about 10^{17} photons. Since radial diffusion is fast in the time required to flow through this region of the cell, in effect these photons are spread across the cell area of 100 cm^2. As noted above, the absorption cross-section of N_2O is 9×10^{-20} cm^2. Thus, on average ~1/10000 N_2O molecules are dissociated per pulse. At a pulse repetition rate of 10 Hz, an N_2O molecule is exposed to 100 pulses before exiting the observation zone at which point approximately 1% of the N_2O molecules will have been dissociated by the laser and typically half that many will have reacted with $O(^1D)$ so that in total about 1.5% of the N_2O is depleted by the far end of the observation zone. The H_2 reagent, which is in comparable concentration to N_2O, will suffer about a 0.5% depletion. Product build-ups from the reaction should be at most in a similar range. It does not seem possible that the factor of 1.8 discrepancy between the observed and expected ratio of slope to intercept in Figure 1a could be explained by reagent depletion or product build-up. This belief was confirmed when essentially the same results were obtained with the pulse repetition rate decreased by a factor of 2.

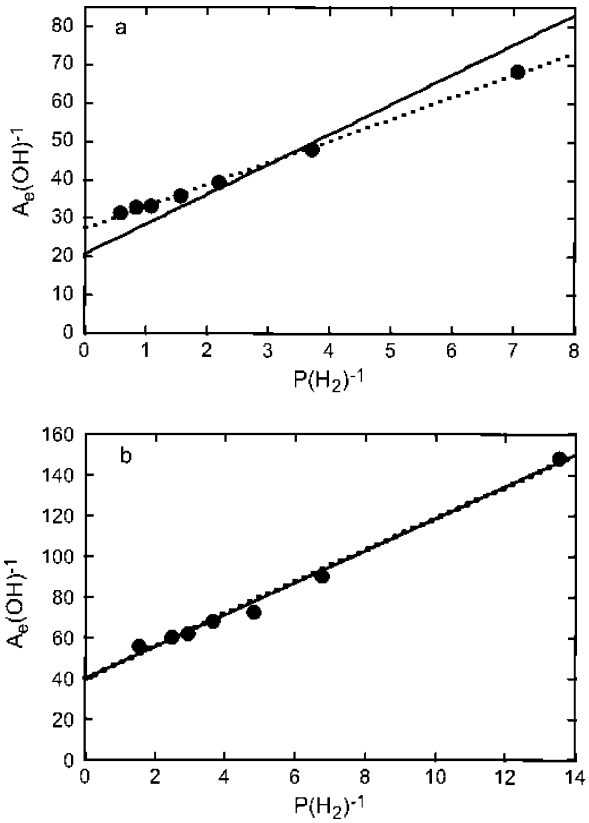

Figure 1. In Figure 1a, $F(He) = 1000$ sccm; $P(He) = 12$ Torr; $F(N_2O) = 30$ sccm; $F(NO) = 4$ sccm; $F(H_2) \sim 10$; 20; 35; 50; 75; 100; 150 sccm. The solid straight line assumes $k(H_2) = 1.1 \times 10^{-10}$, $k(N_2O) = 1.16 \times 10^{-10}$, $k(NO) = 0.6 \times 10^{-10}$ cm^3 $molecule^{-1}$ s^{-1}. The dashed line is the best linear fit of the points. In Figure 1b, $F(He) = 10\,000$ sccm; $P(He) = 63.22$ Torr; the other flows are essentially the same. The solid straight line assumes the rate constants above. The best straight line through the points is indistinguishable from the model line.

The disagreement can also not be caused by secondary chemistry. The only reactions of any significance occurring on short time scale are the vibrational relaxations of vibrationally excited OH. On a longer time scale (about 1 ms), OH reacts with CH_4 producing CH_3 and H_2O. On a similar time scale, OH reacts with NO in a three body process to produce HONO. As described earlier, the reaction between OH and CH_3 takes about 2 ms under our conditions. CH_3, which is not being measured here, also reacts with NO in a three body process to produce CH_3NO. By the extrapolation of the OH signal to $t = 0$, the decay of OH resulting from these slow reactions is removed.

TABLE 1: Rate Constants Used for Analyzing and Modeling the Experimental Stern−Volmer Plots

no. reaction	k ($\times 10^{-10}$ cm^3 molecule^{-1} s^{-1})	ref
(1) $O(^1D) + CH_4 \rightarrow$ products	1.5	8
(1′) $O(^1D) + CD_4 \rightarrow$ products	1.43	this work relative to (2)
(4) $O(^1D) + N_2O \rightarrow$ products	1.16	8
(5) $H + NO_2 \rightarrow OH + NO$	1.3	8
(6) $O(1D) + H_2 \rightarrow H + OH$	1.1	8
(6′) $O(^1D) + D_2 \rightarrow D + OD$	1.1	this work relative to (2)
(7) $O(^1D) + NO \rightarrow$ products	0.6	this work (estimate)
(8)$OH(v>0) + CH_4 \rightarrow OH$ (v=0) + CH_4	0.005	24
(9)$OH(v=1) + NO \rightarrow OH$ (v=0) + NO	0.38	26
(10)$O(^1D) + NO_2 \rightarrow$ products	1.3	this work relative to (4)
(11′) $OD + CD_3CDO \rightarrow D_2O + CD_3CO$	0.16	19
(12) $O(^1D) + CD_3CDO \rightarrow$ products	3	19
(13) $CH_3 + NO_2 \rightarrow CH_3O + NO$	0.33	36
(14) $CH_2OH + NO_2 \rightarrow$ products	0.08	32

It occurred to us that the disagreement might be the result of hot atom chemistry. The photolysis of N_2O at 193 nm can produce $O(^1D)$ with a maximum translational energy of 166 kJ/mol. We estimate using a hard sphere collision model a fractional translational energy loss per collision with He of about 1/3. At a helium flow rate of 1,000 sccm (with a total pressure of about 12Torr in the cell), as many as one in 10 collisions will be with H_2 at the highest H_2 pressures used so that some effects caused by translationally hot $O(^1D)$ seem quite possible under the conditions of Figure 1a. Figure 1b shows a Stern−Volmer plot of the same system with the helium flow rate raised 10-fold with the flow rates of the reagents fixed. From eq I, this increases the ratio of the helium concentration to the concentrations of the other reagents by a factor of 10 providing on average 10-fold more translational energy quenching collisions for an $O(^1D)$ before it collides with a reagent. The agreement with the literature results is excellent. Therefore we concluded that hot atom chemistry does seriously affect reaction rate constants and possibly branching ratios in this system, and we have carried out the quantitative measurements described below at a helium flow rate of 10 000 sccm and a total pressure of about 66 Torr.

The intercept (dotted line) A_e^{-1} value of Figure 1 can be used to estimate $[O(^1D)]_0$ from the known[25] cross-section for the OH line at 3407.989 cm^{-1} ($v = 1 \leftarrow 0$ P(4.5) 1+) and the estimated effective probe laser path length of 20 m. As can be seen from eq III

$$[O(^1D)]_0 = \frac{1}{\sigma L \times \text{intercept}} \qquad \text{(IV)}$$

When the appropriate numbers are substituted into (IV), $[O(^1D)]_0 = 4 \times 10^{12}$ cm^{-3}.

(b) Products. The primary products of reactions 1a−1f are OH, CH_3, H, H_2, H_2CO, CH_3O, CH_2OH, CH_2, and H_2O. H_2O (in the form of D_2O for reasons that will be explained), OH, CH_3, H_2CO, and CH_3O can be directly observed by selected infrared spectral lines. H atoms can be observed indirectly through reaction 5 when NO_2 is used as the $O(^1D)$ precursor. For most of these experiments, $O(^1D) + H_2$ was used as the reference reaction to calibrate the initial $[O(^1D)_0]$. It was assumed that $O(1D) + H_2$ gives exclusively OH + H in 100% yield.

Table 1 lists the rate constants of the reactions using in analyzing and modeling the Stern−Volmer plots.

(i) OH and OD. The main products of the reaction $O(^1D)$ with CH_4 are OH + CH_3. The branching ratio for (1a) was determined by comparing the amount of OH formed by photolysis in the N_2O/CH_4 system with the amount of OH formed by reaction 6 in the N_2O/H_2 system. As mentioned earlier, vibrational relaxation of OH is problematic. OH ($v>0$) is relaxed primarily by CH_4 in the $He/N_2O/CH_4$ system, however, this relaxation is rather slow[24]

$$OH(v = 1) + CH_4 \rightarrow OH(v = 0) + CH_4$$
$$k = 5.2 \times 10^{-13} \text{ cm}^3 \text{ molecule}^{-1} \text{ s}^{-1} \qquad \text{(8a)}$$
$$OH(v = 2) + CH_4 \rightarrow OH(v = 1) + CH_4$$
$$k = 1.7 \times 10^{-12} \text{ cm}^3 \text{ molecule}^{-1} \text{ s}^{-1} \qquad \text{(8b)}$$

By adding NO (~50mTorr) in these experiments, the vibrationally excited OH can be relaxed by reaction 9

$$OH(v = 1) + NO \rightarrow OH(v = 0) + NO$$
$$k = 3.8 \times 10^{-11} \text{ cm}^3 \text{ molecule}^{-1} \text{ s}^{-1} \qquad \text{(9)}$$

with a time constant of about 16 μs.[26]

Because the reactions 4 and 7 consume a fraction of the $O(^1D)$, the relative product concentration must be determined from the intercepts of Stern−Volmer plots. To determine the branching ratio $\alpha = k_{1a}/k_1$, two plots of the inverse of OH absorbance (base e) versus the inverse of reactant partial pressure (for one plot CH_4, for the other H_2) were made, and the points were fitted with a straight line. The concentrations $[CH_4]$ (or $[H_2]$), $[N_2O]$ and [NO] remain essentially constant throughout the reaction, therefore

$$\frac{1}{[OH]_{0,1}} = \frac{k_1}{k_{1a}[O(^1D)]_0}\left(1 + \frac{k_4[N_2O] + k_7[NO]}{k_1[CH_4]}\right) \qquad \text{(V)}$$

where $[OH]_{0,1}$ is the OH concentration produced by reaction 1 and corresponds to the longer term OH signal extrapolated back to $t = 0$. When using H_2, we have a similar expression (II). The OH absorbance signal (base e) extrapolated to $t = 0$, $S°$-([OH]), is proportional to $[OH]_0$, therefore, since $[N_2O]$ and [NO] were unchanged

$$\alpha = k_{1a}/k_1 = \frac{\text{intercept } (H_2 \text{ with } N_2O)}{\text{intercept } (CH_4 \text{ with } N_2O)} \qquad \text{(VI)}$$

Figure 2 shows time traces of the OH signal for the H_2 and the CH_4 systems. Figure 3 shows the Stern−Volmer plots resulting from these signals. From the ratio of the intercepts of this plot, the value of α obtained is 0.67.

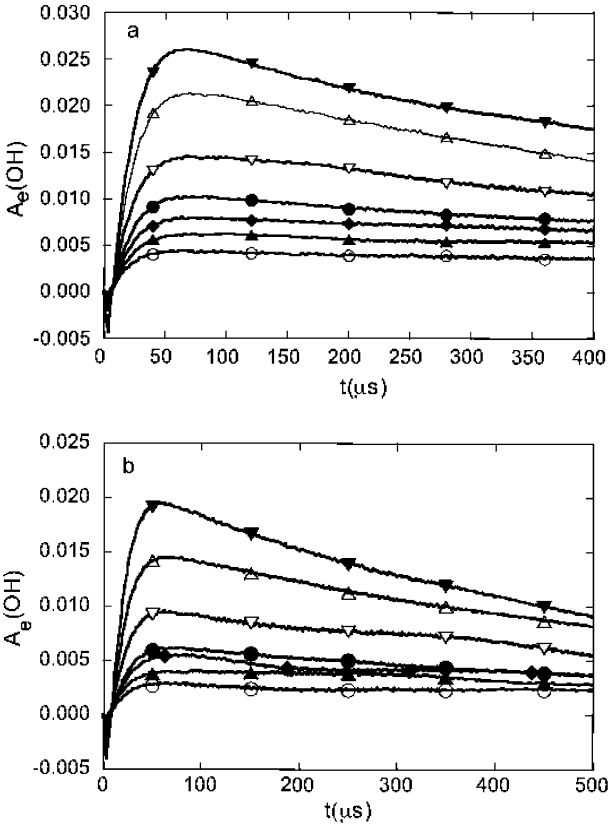

Figure 2. Time traces of the OH signal at 3407.989 cm^{-1} ($1 \leftarrow 0$ P(4.5) 1 + transition) for the H_2 and the CH_4 systems. In Figure 2a, F(He) = 10 000 sccm; P(He) = 65 Torr; $F(N_2O)$ = 60 sccm; $P(N_2O)$ ~ 0.394 Torr; F(NO) = 8 sccm; P(NO) ~ 0.053 Torr. $F(H_2)$ ~ 6.3 (○); 8.4 (▲); 11.5 (♦); 16.7 (●); 27.2 (▽); 53.2 (△);102.7 (▼) sccm. In Figure 2b, $F(CH_4)$ ~ 6.8 (○); 8.8 (▲); 11.9 (♦); 17.2 (●); 28.1 (▽); 54.8 (△); 105.9 (▼) sccm. Other conditions are the same as Figure 2a.

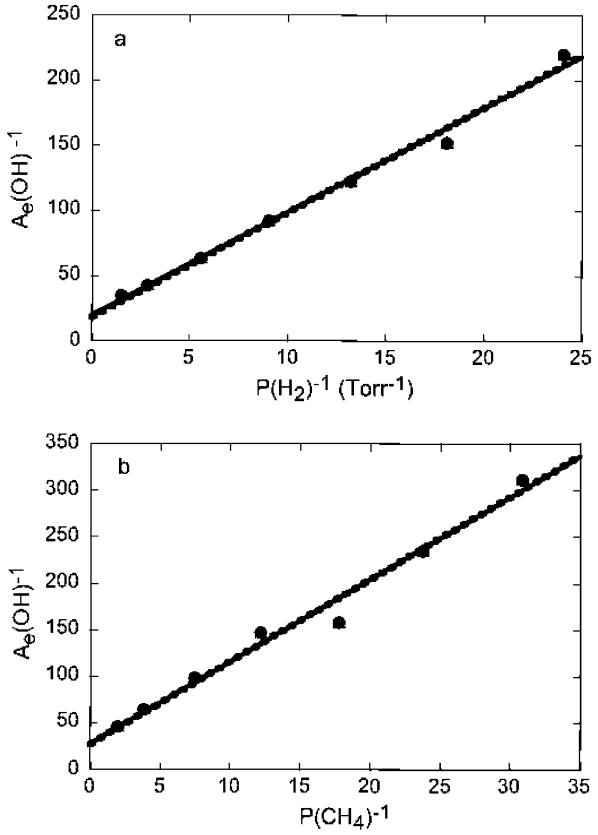

Figure 3. Stern−Volmer plots resulting from Figure 2. In Figure 3a, the solid straight line assumes $k(H_2) = 1.1 \times 10^{-10}$, $k(N_2O) = 1.16 \times 10^{-10}$, k(NO) = 0.6×10^{-10} cm^3 $molecule^{-1}$ s^{-1}. Its intercept is 18.21. The dashed line is the best linear fit of the points, which is indistinguishable from the model line when plotted to this scale. In Figure 3b, the solid straight line assumes the rate constants above, with $k(CH_4)$ 1.5×10^{-10} cm^3 $molecule^{-1}$ s^{-18}, and its intercept is 27.38.

Of course, the Stern−Volmer plot shown in Figure 3 is not the only set of data obtained. In the fitting of multiple datasets, an issue of consistency arises, because the ratio of the intercept to slope is fixed by the ratio of rate constants. Therefore, it did not make sense in fitting each dataset to allow the slope and intercept to vary independently. Instead the overall rate constants were fixed to values in the JPL evaluation,[8] and the Stern−Volmer plots were fitted with a single adjustable parameter. The average of several experiments gives 67% yield of OH. The uncertainties in the rate constants in the evaluation are large enough to affect the branching ratios. For example, the recommended rate constant of reaction 6 is 1.1×10^{-10} cm^3 $molecule^{-1}$ s^{-1} in the JPL evaluation. A rate constant for this reaction of 1.2×10^{-10} cm^3 $molecule^{-1}$ s^{-1} seems equally plausible to us. Substituting the latter rate constant in the fitting causes the branching ratio α to increase by 5% to about 0.72.

With CH_4 replaced by CD_4 and H_2 replaced by D_2, the OD yield is measured using the same strategy. OD signals were observed at[27] 2710.1418 cm^{-1} ($v = 1 \leftarrow 0$ $R_{1e}(3.5)$) for the N_2O/D_2 and N_2O/CD_4 systems. Figure 4 shows the Stern−Volmer plots resulting from these signals. The resulting value of α_D obtained from Figure 4, parts a and b, is 0.58 assuming that k_{6D} ($\equiv k_{6'}$) is 1.1×10^{-10} cm^3 $molecule^{-1}$ s^{-1} and k_{1D} ($\equiv k_{1'}$) is 1.43×10^{-10} cm^3 $molecule^{-1}$ s^{-1}. An appropriate average of all data gives the OD yield as 60 ± 5%.

(ii) H&D. $O(^1D)$ can also be produced from photolyzing NO_2 at 193 nm by excimer laser. When N_2O is replaced by NO_2, the atom H or D from reaction 1 or 6 will convert into OH or OD through reaction 5. Here the reaction

$$O(^1D) + NO_2 \rightarrow \text{products} \qquad (10)$$

also consumes $O(^1D)$.

As mentioned earlier, there is much more secondary chemistry when NO_2 is used as the source for $O(^1D)$ than with N_2O. For many purposes, this secondary chemistry could cause a problem but not for the measurement of OH. The time profiles of the OH signal of the H_2 and CH_4 systems are remarkably similar. Ultimately, the quantity of importance is the ratio of the CH_4 to H_2 signal. The similarity between the H_2 and CH_4 time profiles helps to ensure that extrapolation to zero time presents no problem. The rapid achievement of maximum signal is the result of the large rate constants of reactions 1 and 5 and the rapid relaxation of vibrationally excited OH by NO_2. The decay of OH is dominated by the three body reaction between OH and NO_2 to form HNO_3.

Making the same S−V plots as above, we compare the intercept of the CH_4 system to that of the H_2 system to obtain the sum of the direct OH yield and the H atom yield. This is expressed by the equation below

$$R = 2\frac{\text{Intercept } (H_2 \text{ with } NO_2)}{\text{intercept } (CH_4 \text{ with } NO_2)} = 2\frac{k_{1a} + k_{1b} + k_{1c} + 2k_{1e}}{2k_1} \qquad \text{(VII)}$$

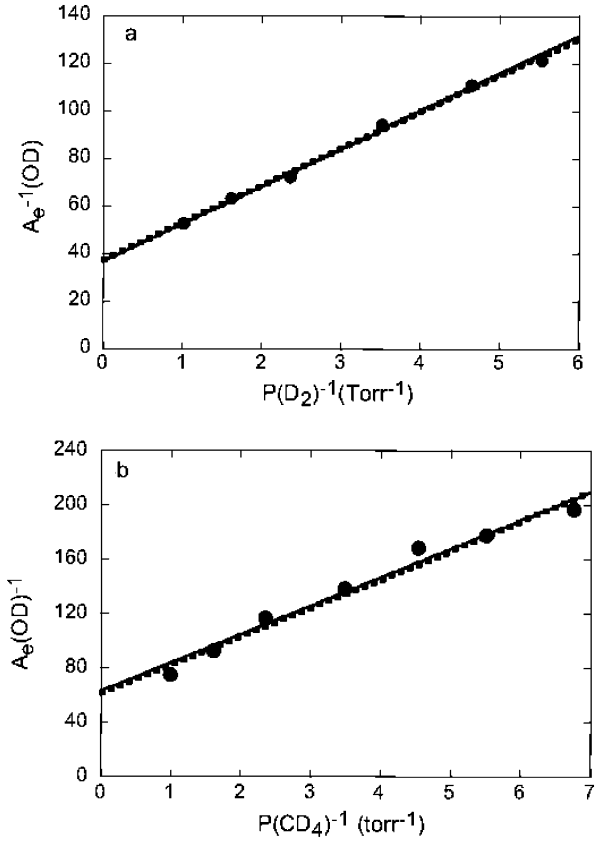

Figure 4. Stern−Volmer plots of OD in N_2O/D_2 and N_2O/CD_4 system. The OD signals were observed at 2710.1418 cm^{-1}. In Figure 4a, F(He) = 10 000 sccm; P(He) ∼ 63 Torr; $F(N_2O)$ = 60 sccm; $P(N_2O)$ ∼ 0.387 Torr; F(NO) = 8 sccm; P(NO) ∼ 0.052 Torr. $F(D_2)$ ∼ 22.6; 28.1; 33.4; 44.2; 65.8; 96.7; 153.9 sccm. In Figure 4b, $F(CD_4)$ ∼ 22.9; 28.1; 34.1; 44.4; 65.7; 95.9; 154.7 sccm. Other conditions are the same as Figure 4a. Figure 4a, assumes $k(N_2O) = 1.16 \times 10^{-10}$, k(NO) = 0.6 × 10^{-10} cm^3 molecule^{-1} s^{-1}, and $k(D_2)$ is determined to be ∼1.1 × 10^{-10} cm^3 molecule^{-1} s^{-1}. The intercept for the fitting line is 36.55. In Figure 4b, the intercept for the fitting is 62.59. $k(CD_4)$ is determined to be 1.43 × 10^{-10} cm^3 molecule^{-1} s^{-1}.

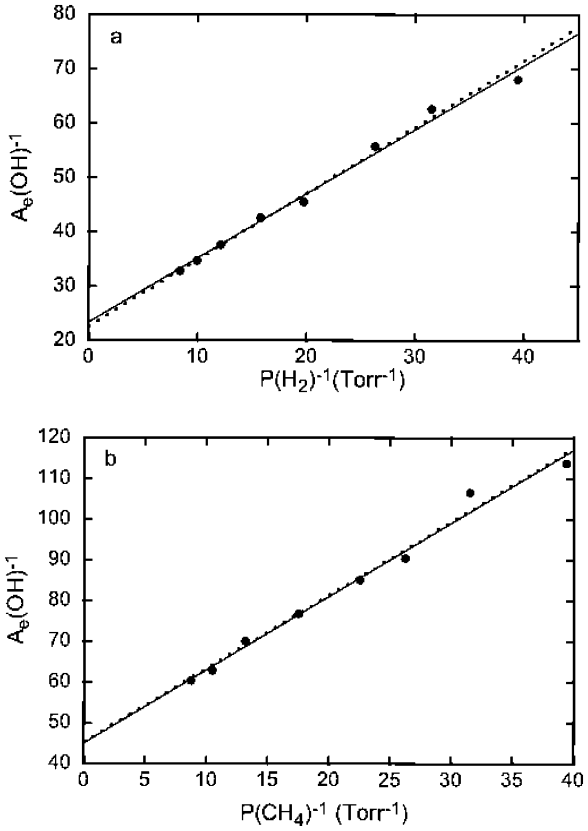

Figure 5. Stern−Volmer plots for the OH signals at 3407.989 cm^{-1} of both the H_2 and CH_4 in NO_2 systems. In Figure 5a, F(He) = 10000 sccm; P(He) = 63.5 Torr; $F(NO_2)$ = 7.2 sccm; $P(NO_2)$ ∼ 0.0459 Torr; $F(H_2)$ ∼ 19; 16; 13; 10; 8; 6; 5; 4 sccm. In Figure 5b, $F(CH_4)$ ∼ 18; 15; 12; 9; 7; 6; 5; 4 sccm. Other conditions are the same as Figure 5a. The solid straight lines are the best linear fits of the points. Assuming that $k(H_2) = 1.1 \times 10^{-10}$, $k(CH_4) = 1.5 \times 10^{-10}$ cm^3 molecule^{-1} s^{-1}, $k(NO_2)$ is determined from all of our data to be 1.30 × 10^{-10} cm^3 molecule^{-1} s^{-1}. The dashed lines are the modeling results using this number with this data set. The intercepts are 22.57 for Figure 5a and 45.29 for Figure 5b.

When eqs VI and VII are combined, the branching ratio for H atom can be expressed as

$$\beta = k_{1H}/k_1 = \frac{2 \times \text{intercept } (H_2 \text{ with } NO_2)}{\text{intercept } (CH_4 \text{ with } NO_2)} - \frac{\text{intercept } (H_2 \text{ with } N_2O)}{\text{intercept } (CH_4 \text{ with } N_2O)}$$

$$= R - \alpha \qquad \text{(VIII)}$$

where the total rate constant for production of OH atoms is $k_{1H} = k_{1b} + k_{1c} + 2k_{1e}$. Figure 5 shows Stern−Volmer plots of OH signals observed in the NO_2/H_2 and NO_2/CH_4 system. Assuming that $k_6 = 1.1 \times 10^{-10}$, $k_1 = 1.5 \times 10^{-10}$ cm^3 molecule^{-1} s^{-1}, the rate constant of reaction 10 is determined to be is 1.3 × 10^{-10} cm^3 molecule^{-1} s^{-1}(the details will be discussed later at 3c). R was estimated as 0.99 from the ratio of the two intercepts. Figure 6 shows the Stern−Volmer plots for the corresponding deuterium system. These plots yield R_D = 0.96 from the ratio of intercepts.

Other measurements of R are as low as 0.91, and there are even higher measurements well above 1, and there is a similar scatter in R_D. The estimated variation in the average is about ±0.1 somewhat larger than the variations in α, which range to about ±0.05. Table 2 shows several measurements of OH and OD yields in the case of photolyzing N_2O and NO_2 as O(^{1}D) sources. The final value of β is 0.3 ± 0.1 taking into account the uncertainties in both R and α. The final value of β_D is 0.3$_5$ ± 0.1.

(iii) D_2O. When we first observed D_2O signals by photolyzing N_2O and CD_4, we considered the possibility that D_2O might come from the reaction of vibrationally excited OD with CD_4. We investigated this possibility by searching for prompt signals from HDO in a 50−50% mixture of CH_4 and CD_4. If no HDO is produced on the time scale of reaction 1, prompt D_2O signals in the purely deuterated system arising from secondary reactions can be ruled out. To carry this comparison out, HDO signals were observed at[25] 2779.9630 cm^{-1}. The integrated line strength of this line can be calculated as 3.02 × 10^{-20} cm from the HITRAN 2000[25] value of 9.41 × 10^{-24} cm at the D atom natural abundance 0.00031069. In comparison, D_2O signals were observed at[28] 2711.2171 cm^{-1} ($\nu_3 = 5_{14} \leftarrow 6_{15}$). We have measured the integrated line strength of this line to be 2.68 × 10^{-20} cm using pure D_2O in a short cell. Note these two lines have comparable line strengths.

Figure 7 shows that very little HDO is formed at reaction times of less than 40 μs in the $N_2O/CD_4/CH_4$ system. For comparison, a D_2O time trace recorded in the N_2O/CD_4 system is also shown. It is clear that the early time behavior of the two traces is entirely different. In the CD_4 only system, D_2O rises

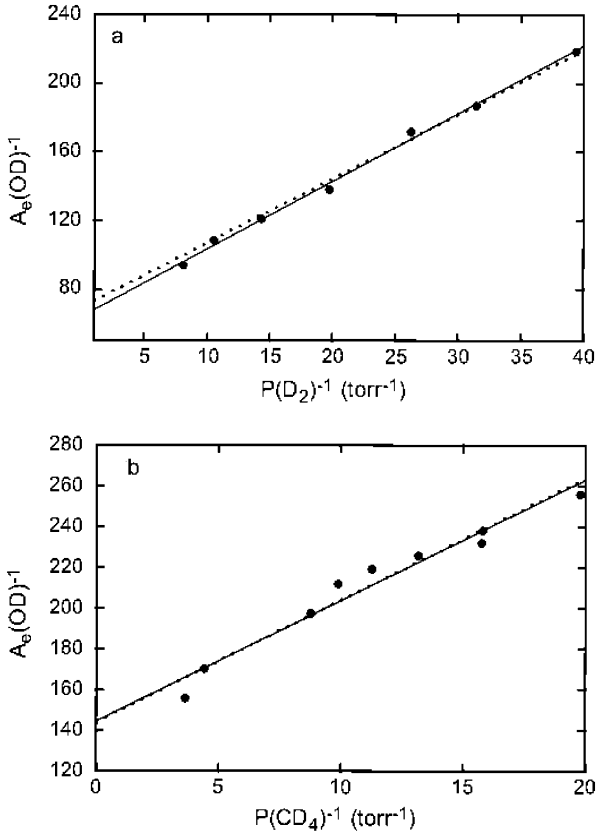

Figure 6. OD Stern−Volmer plots in both $D_2 + NO_2$ and $CD_4 + NO_2$ system. In Figure 6a, F(He) = 10 000 sccm; P(He) ~ 63.0 Torr; $F(NO_2)$ = 7.2 sccm; $P(NO_2)$ ~ 0.046 Torr; $F(D_2)$ ~ 4.0; 5.0; 6.0; 8.0; 11.0; 15.0; 19.5 sccm. The intercept for the modeling fitting line is 69.38, while supposing $k(D_2) = 1.1 \times 10^{10}$ and $k(NO_2) = 1.30 \times 10^{-10}$ cm^3 molecule^{-1} s^{-1}. In Figure 6b, $F(CD_4)$ ~ 8.0; 10.0; 10.0; 12.0; 14.0; 16.0; 32.0; 32.2; 40.0 sccm. The other flows are the same as Figure 9a. The intercept for the modeling fitting line is 144.05, while supposing $k(CD_4) = 1.43 \times 10^{-10}$ and $k(NO_2) = 1.30 \times 10^{-10}$ cm^3 molecule^{-1} s^{-1}. The best linear fitting lines are superimposed together with modeling lines at the both cases. Again the dashed lines are the modeling results.

TABLE 2: Measurements of OH and OD Yields[a]

	OH yield		OD yield	
No	$N_2O/CH_4/NO/He$ α_H	$NO_2/CH_4/He$ R_H	$N_2O/CD_4/NO/He$ α_D	$NO_2/CD_4/He$ R_D
1	0.67	0.99	0.58	0.96
2	0.64	1.07	0.64	0.91
3	0.73	0.98	0.59	0.98
4	0.67	0.92		
av	0.68	0.98	0.60	0.95

[a] Experimental detail and the methodology of data processing are described at 3b(i) and (ii). Experimental conditions of no. 1 are shown in the captions of Figure 2−6. Measurements 2−4 have similar conditions to those of no. 1.

rapidly at first (until about 40 μs) but then rises much more slowly. For the HDO signal in the mixed isotope system, only the slow rise occurs, with "slow" HDO formation proceeding about twice as rapidly as "slow" D_2O formation in the CD_4 only system, because the OD + CH_4 reaction is about seven times faster than the OD + CD_4 reaction[29] and thus makes a significant contribution to HDO production. It is very difficult to explain the early D_2O formation on any basis other than direct production of D_2O by reaction 1.

Another way to verify this conclusion is by adding NO to the N_2O/CD_4 system. Figure 7 also shows the comparison of

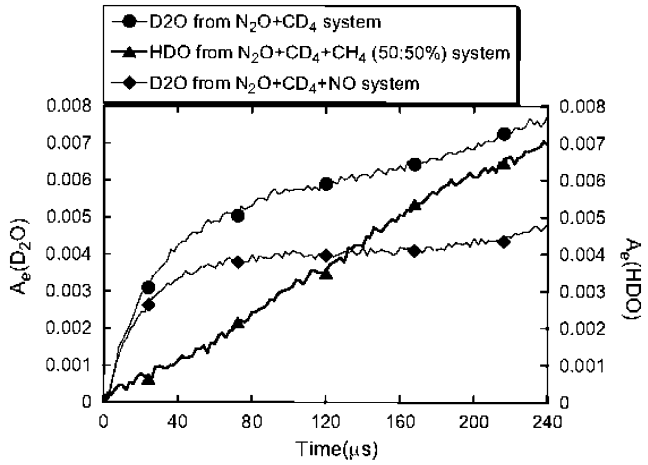

Figure 7. HDO time trace (▲) photolyzing $N_2O/CH_4/CD_4$. F(He) = 1000 sccm; $F(N_2O)$ = 30 sccm; $F(CH_4)$ = 50 sccm; $F(CD_4)$ = 50 sccm; P(tot) = 13.56 Torr. The comparison D_2O signals at 2711.2127 cm^{-1} in the CD_4, N_2O system are shown with NO and without NO. F(He) = 1000 sccm and P(He) = 12 Torr. $F(CD_4)$ = 50 sccm; $F(N_2O)$ = 30 sccm; ●, without NO; ♦, with 11 sccm NO.

D_2O signals in the CD_4 only system obtained with and without NO. We can see that the early rising signals (before 40 μs) in both cases are almost the same. The similarity between D_2O production with and without NO shows that the prompt D_2O cannot be formed by reactions of vibrationally excited OD because 98% of OD(v = 1), 92% of OD(v = 2), and 84% of OD(v = 3) should have been relaxed within 25 μs by NO when it was added to the reaction mixture.[24,26] At longer times the with and without NO signals diverge. The added NO must be removing the reagent responsible for the slowly rising D_2O signal.

The water yield was quantified by a scheme similar to that used for the OH yield. Since the IR beam passes through perhaps a meter of air and would be greatly attenuated by atmospheric water on H_2O absorption lines, we chose to create D_2O in the presence of CD_4 observing the D_2O line[28] at 2711.2127 cm^{-1} ($\nu_3 = 5_{14} \leftarrow 6_{15}$; $E'' = 279.56$ cm^{-1}) using the reaction

$$O(^1D) + CD_4 \rightarrow D_2O + CD_2 \qquad (1f')$$

in combination with the following reference system to produce a known amount of D_2O

$$O(^1D) + D_2 \rightarrow D + OD \qquad k_{6'} = 1.1 \times 10^{-10}\ \text{cm}^3\ \text{s}^{-1} \quad (6')$$

$$OD + CD_3CDO \rightarrow D_2O + CD_3CO \qquad k_{11'} = 1.6 \times 10^{-11}\ \text{cm}^3\ \text{s}^{-1} \quad (11')$$

In the reference system, a slight allowance must be made for the complication caused by

$$O(^1D) + CD_3CDO \rightarrow \text{products} \qquad k_{12'} = 3 \times 10^{-10}\ \text{cm}^3\ \text{s}^{-1} \quad (12')$$

since the products of reaction 12′ may include D_2O and/or OD, which results in D_2O. In the following analysis, we call the sum of these channels 12a′.

Since the D_2O yield from (11′) is almost 100%[19] and reaction 11 is fast (1.67×10^{-11} cm^3 s^{-1}), we can compare the D_2O absorbance from the CD_4/N_2O system with the D_2O absorbance from the $D_2/N_2O/CD_3CDO$ system to obtain the D_2O yield for the title reaction. As D_2O is stable and exchanges only slowly,

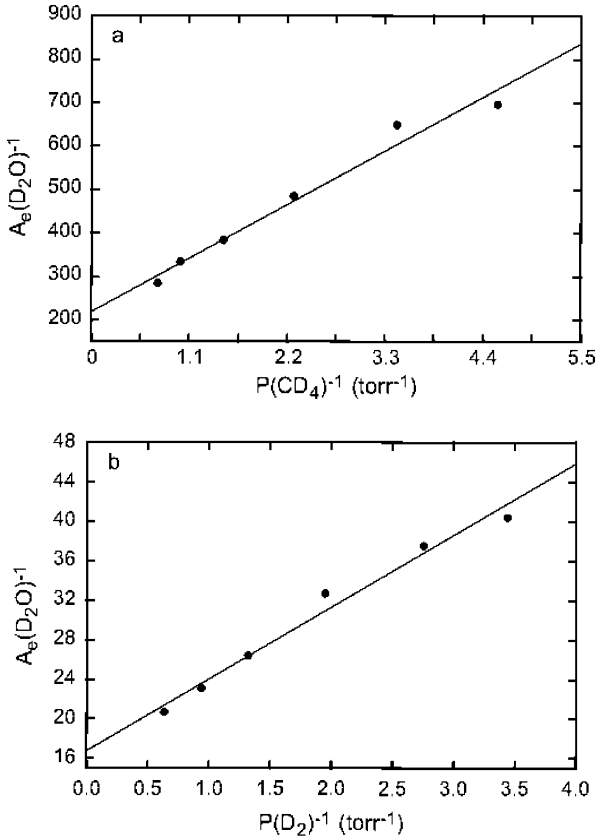

Figure 8. D_2O S−V plots observed at 2711.2127 cm^{-1} produced in the CD_4, N_2O system (8a) and the D_2, CD_3CDO, N_2O system (8b). F(He) = 10 000 sccm; P(He) = 64.5 Torr; $P(N_2O) \sim 0.537$ Torr. In Figure 8a, $F(CD_4) \sim$ 30; 40; 60; 90; 130, 170 sccm. In Figure 8b, $F(D_2) \sim$ 40; 50; 70; 102; 140; 200 sccm, $F(CD_3CDO) \sim 1.85$ sccm. In the CD_4, N_2O system, the intercepts of linear fitting from 20 to 40 μs signals are assumed to be D_2O_∞ from $O(^1D) + CD_4$. The slow rising parts are assumed to be from $OD + CD_4$. In the D_2, CD_3CDO, N_2O system, the signals of D_2O_∞ from $OD + CD_3CDO$ are taken from the 1.2 ms signals. The intercepts of S−V plots in the two cases are (8a) 221.19 and (8b) 16.89, giving γ_D 0.076.

we can use its signal after reaction (11′) has reached completion. Consider the Stern−Volmer plots for the two sets of measurements. In analogy to (III) we have

$$\frac{1}{[D_2O]_{1f'}} = \frac{k_{1'}}{k_{1f'}[O(^1D)]_0}\left(1 + \frac{k_4[N_2O]}{k_{1'}[CD_4]}\right) \qquad \text{(IX)}$$

The similar equation from the combination of reactions 6′, 11, 12′, and 12a′ is

$$\frac{1}{[D_2O]_{ref}} = \frac{1}{[O(^1D)]_0}\left(1 + \frac{k_4[N_2O] + k_{12'}[CD_3CDO]}{k_{6'}[D_2] + k_{12a'}[CD_3CDO]}\right) \qquad \text{(X)}$$

Since we made $k_{6'}[D_2] \gg k_{12a'}[CD_3CDO]$, the term $k_{12a'}[CD_3CDO]$ can be neglected, and we can make a Stern−Volmer plot for $1/S_{D_2O}$ vs $1/[D_2]$. The D_2O yield for reaction 1′ is then

$$\gamma_D = k_{1f'}/k_{1'} = \frac{\text{intercept } (D_2 \text{ with } N_2O \text{ and } CD_3CDO)}{\text{intercept } (CD_4 \text{ with } N_2O)} \qquad \text{(XI)}$$

Figure 8a shows the Stern−Volmer plot from the N_2O/CD_4 system, and Figure 8b shows the plot from the $N_2O/D_2/CD_3CDO$ system. The resulting value of γ_D is 0.076 or an 8% yield of D_2O.

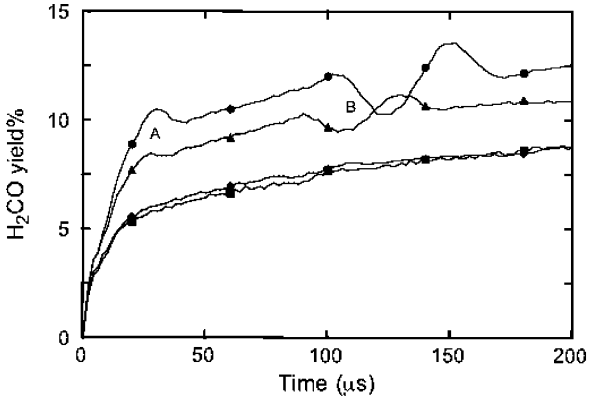

Figure 9. H_2CO signals in the N_2O and CH_4 system, while H_2CO absorbances have been converted to % yield of H_2CO. Experimental parameters are $F(N_2O)$ = 60 sccm; F(NO) = 8 sccm (for relaxing the vibrationally excited OH); $F(CH_4)$ = 100 sccm. The signals are recorded at 4 different pressures of buffer gas helium. ●, F(He) = 500 sccm, P(He) ~ 7 Torr; P(total) ~ 10 Torr; ▲, F(He) = 1000 sccm, P(He) ~ 12 Torr; P(total) ~ 14.22 Torr; ♦, F(He) = 3000 sccm, P(He) ~ 25.5 Torr, P(total) ~ 27.9 Torr; ■, F(He) = 5000 sccm, P(He) ~ 37.2 Torr, P(total) ~ 39.5 Torr. There are shock-waves at the locations indicated by the letters A and B for 500 and 1000 sccm helium flow. From the figure, we can see that the yields of H_2CO seem to be dependent on the pressure of the helium buffer gas. At 20 ms, the yields of H_2CO are 5.5%, 5.8%, 8.4%, and 10.2% at P(He) of 37.2, 25.5, 12, and 7 Torr, respectively.

(iv) H_2CO. Formaldehyde is produced through (1d) and (1e). By comparing OH absorbance with H_2CO absorbance upon photolysis of the N_2O/CH_4/He system, the yield of H_2CO from the title reaction can be calculated. The H_2CO line[25] at 2831.6417 cm^{-1} (line strength $S^0_{HCHO} = 5.04 \times 10^{-20}$ cm molecule^{-1}; line width δ_{HCHO} = 116 MHz) was chosen for comparison with the OH line at 3407.989 cm^{-1} (line strength $S^0_{OH} = 4.7204 \times 10^{-20}$ cm molecule^{-1}; line width δ_{OH} = 185 MHz). Then

$$\text{yield}_{HCHO} = \text{yield}_{OH}\frac{S_{HCHO\infty}}{S_{OH\infty}}\frac{S^0_{OH}}{S^0_{HCHO}}\frac{\delta_{HCHO}}{\delta_{OH}} = 0.587\ \text{yield}_{OH}\frac{S_{HCHO\infty}}{S_{OH\infty}} \qquad \text{(XII)}$$

Measurements of OH and H_2CO signals were made for four different buffer gas pressures (with 7, 12, 25.5, and 37.2 Torr Helium pressure). In Figure 9, the H_2CO absorbance has been converted into yield % according to (XII) using line widths for OH and H_2CO that were obtained directly from our fitting procedure. We deduce the value of $\delta = (k_{1d} + k_{1e})/k_1$ in the absence of hot atom effects as 5%.

The significance of the increased yields of CH_2O at low pressure is not certain. A possibly plausible suggestion is that the additional translational energy of $O(^1D)$ at low pressure leaves more energy in the highly excited CH_3OH dissociating intermediate increasing the three body breakup ($CH_2O + H + H$) yield.

(v) CH_3O and CH_2OH. A search was carried out for the CH_3O radical. When CH_4/NO_2 mixtures were photolyzed, we observed the absorption spectrum of CH_3O radical around 2866 cm^{-1} previously reported by Han et al.[30] However, it is most likely produced from the reaction[31]

$$CH_3 + NO_2 \rightarrow CH_3O + NO \qquad (13)$$

Upon photolysis of the N_2O/CH_4/He system, no CH_3O absorption lines were observed. As the CH_3O cross-sections are

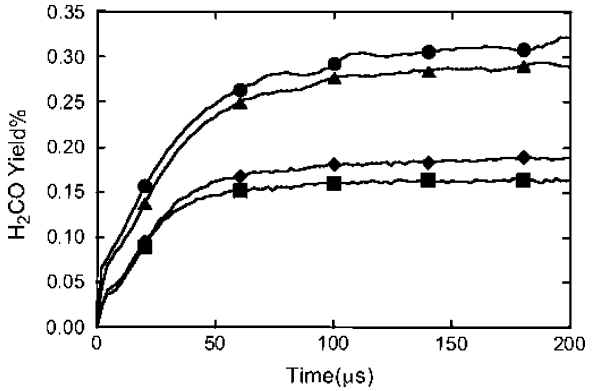

Figure 10. H_2CO signals in the NO_2 and CH_4 system, while H_2CO absorbances have been converted to % yield of H_2CO. Experimental parameters are $F(NO_2) = 7.2$ sccm; $F(CH_4) = 30$ sccm. The signals are recorded at 4 different pressures of buffer gas helium. ●, $F(He) =$ 500 sccm, $P(total) \sim 8.17$ Torr; ▲, $F(He) = 1000$ sccm, $P(total) \sim$ 12.4 Torr; ♦, $F(He) = 3000$ sccm, $P(total) \sim 25.85$ Torr; ■, $F(He) =$ 5000 sccm, $P(total) \sim 37.54$ Torr.

unknown, it is not possible to put an upper limit on channel 1c from this negative result.

Some years ago, we observed a complex, weak spectrum near 3600 cm^{-1} that we believed belonged to CH_2OH, but we remain doubtful of this assignment. A search was carried out in the region of this spectrum, and no lines were observed.

Despite these negative results, some information concerning the formation of CH_2OH and CH_3O was obtained by comparing formaldehyde time traces obtained using CH_4/NO_2 mixtures with those obtained using CH_4/N_2O mixtures. As can be seen from Figure 10, the amount of formaldehyde formed in the presence of NO_2 (expressed as a percentage of the original $O(^1D)$ concentration) is 3−4 times greater than that formed by photolyzing CH_4/N_2O mixtures. In addition, the time behavior of the two traces is different. In the presence of NO_2, the formaldehyde signal rises fairly smoothly, reaching its maximum value in about 75 μs. Thereafter, it remains more or less constant. In contrast, the signal recorded when using N_2O as the $O(^1D)$ source, rose rapidly for the first 20 μs and then much more slowly for the next 200−300 μs.

We can attribute the extra yield observed in the presence of NO_2 (about 12%) to formaldehyde formed by the reaction

$$CH_2OH + NO_2 \rightarrow CH_2O + HNO_2 \text{ (or } OH + NO) \quad (14)$$

The rate constant for this reaction has been measured as 8×10^{-12} cm^3 $molecule^{-1}$ s^{-1} and formaldehyde has been reported to be a reaction product.[32] Under our conditions, this reaction would produce formaldehyde on a time scale consistent with our observations ($\tau = 43$ μs). No alternative source of the extra CH_2O seems feasible. An alternative source might be the reaction of CH_3 with NO_2. However, at least 97% of the CH_3 produced reacts with NO_2 to form $CH_3O + NO$, CH_3O reacts with NO_2 primarily by a three body reaction that forms an adduct, with less than 3% of the reaction occurring via a bimolecular reaction to form CH_2O,[33] and no other carbon-containing radicals are formed in 12% yield. In the experiments performed using N_2O, the early CH_2O can be attributed to the direct reaction of $O(^1D)$ with CH_4, whereas the small amount formed at later times can be attributed to the reaction of CH_2-OH with NO (which was added to these mixtures to aid vibrational relaxation) or to radical−radical reactions.

(c) Measurement of the Rate Constants of Reactions 1 and 10 Relative to Reaction 4. The direct measurement of the rate constant of reaction 1 is beyond our capabilities. However, analysis of the Stern−Volmer plots of Figure 3 yields the rate constant of reaction 1 relative to that of reaction 4. From eq V, the ratio of the intercept to the slope of the Stern−Volmer plots is

$$\frac{\text{intercept}}{\text{slope}} = \frac{k_1}{k_4[N_2O] + k_5[NO]} \quad \text{(XIII)}$$

The concentration of NO is much less than that of N_2O and $k_5 < k_4$ so that (XIII) essentially measures k_1/k_4. Including the contribution from the NO reaction and using the rate constants k_4 and k_5 given before, we obtain $k_1 = 1.5 \times 10^{-10}$ $molecules^{-1}$ cm^3 s^{-1}. This is in excellent agreement with the value chosen for the JPL compilation.[8]

By using the same strategy, we can determine the rate constant k_{10} of $O(^1D) + NO_2$ under thermalized condition. From Figure 5, assuming that $k_6 = 1.1 \times 10^{-10}$ and $k_1 = 1.5 \times 10^{-10}$ cm^3 $molecule^{-1}$ s^{-1}, k_{10} is determined to be 1.3×10^{-10} cm^3 $molecule^{-1}$ s^{-1} with excellent agreement between the value found using H_2 and that using CH_4. If the two cases gave *exactly* the same rate constant for the reaction of NO_2 with $O(^1D)$, the solid and dashed curves would be superimposed in both parts a and b of Figure 5. From Figures 4 and 6, we can also determine the rate constants of the deuterated systems $k_{6'}$ and $k_{1'}$ for $O(^1D) + D_2$ and $O(^1D) + CD_4$ as $\sim 1.1 \times 10^{-10}$ and 1.43×10^{-10} cm^3 $molecule^{-1}$ s^{-1}, respectively.

TABLE 3: Comparison of Branch Ratios and Product Yields between $O(^1D) + CH_4$ and $O(^1D) + CD_4$

reaction	channel	yields	yields from JPL[8]
$O(^1D) + CH_4$	$OH + CH_3$	67 ± 5%	75 ± 15%
	H + products	30 ± 10%	20 ± 7%
	H_2CO + products	5%	5 ± 5%
	$H_2O + {}^1CH_2$	*a*	not listed
$O(^1D) + CD_4$	$OD + CD_3$	60 ± 5%	
	D + products	35 ± 10%	
	D_2CO + products	a	
	$D_2O + CD_2$	8%	

[a] It was not feasible to measure this quantity in this work.

4. Discussion

As discussed in the Introduction, there have been several measurements of one or more of the branching ratios for this reaction without a very accurate consensus emerging. Table 3 is a summary of our measurements. Our results of (1a) 67%, (1b) + (1c) + 2(1e) 30%, and (1d) + (1e) 5% almost fall within the fairly wide error bounds of the most recent JPL compilation[8] estimates of (1a) (75 ± 15)%, (1b) + (1c) (20 ± 7)%, and (1d) (5 ± 5)%. Presumably in this compilation the value given for (1d) is really the sum (1d) + (1e) as it is hard for the experiments to distinguish these two channels. There has been no previous measurement of the branching into channel (1f). Ignoring the issue that yields change upon deuteration, the sum of the OH, H, CH_2O, and H_2O (substituting the D_2O yield for H_2O) yields is 67 + 30 + 5 + 8 = 110%. Our error bars are large enough that 110% is equivalent to 100%; however, we suspect that channel (1e), although small, could amount to a few percent. We also suspect that channel (1c) producing CH_3O is almost negligible, because we do not observe CH_3O in the N_2O system.

There is general agreement that the mechanism for this reaction is dominated by addition of $O(^1D)$ to CH_4 producing very highly excited CH_3OH that then undergoes very rapid intermolecular decay.[34,35] The lower branching of the deuterated form into channel (1a) and the higher branching of the deuterated

form into D (H) atom channel also appears real. It is unfortunate that experimental problems prevent us from measuring channel (1f) for the normal species and channels (1d) + (1e) for the deuterated system, as a complete knowledge of the isotope effects on the branching ratios would provide theoreticians a fund of information to explain.

Acknowledgment. This work was supported by grants from the Department of Energy and the Robert A. Welch Foundation.

References and Notes

(1) Wiesenfeld, J. R. *Acc. Chem. Res.* **1982**, *15*, 110.
(2) Warneck, P. *International Geophysics Series, Vol. 41: Chemistry of the Natural Atmosphere*, Academic Press: San Diego, 1988.
(3) Fletcher, I. S.; Husain, D. *Can. J. Chem.* **1976**, *54*, 1765.
(4) Schofield, K. *J. Photochem.* **1978**, *9*, 55.
(5) Force, A. P.; Wiesenfeld, J. R. *J. Phys. Chem.* **1981**, *85*, 782.
(6) Gauthier, M. J. E.; Snelling, D. R. *J. Photochem.* **1975**, *4*, 27.
(7) Matsumi, Y.; Tonokura, K.; Inagaki, Y.; Kawasaki, M. *J. Phys. Chem.* **1993**, *97*, 6816.
(8) Sander, S. P.; Friedl, R. R.; Golden, D. M.; Kurylo, M. J.; Huie, R. E.; Orkin, V. L.; Moortgat, G. K.; Ravishankara, A. R.; Kolb, C. E.; Molina, M. J.; Finlayson-Pitts, B. J. *JPL Publication 02-25*; Jet Propulsion Laboratory, California Institute of Technology: Pasadena, CA, 2003.
(9) Atkinson, R.; Baulch, D. L.; Cox, R. A.; Hampson, R. F. J.; Kerr, J. A.; Rossi, M. J.; Troe, J. *J. Phys. Chem. Ref. Data* **1997**, *26(3)*, 521.
(10) Lin, C. L.; DeMore, W. B. *J. Phys. Chem.* **1973**, *77*, 863.
(11) Addison, M. C.; Donovan, R. J.; Garraway, J. *J. Chem. Soc., Faraday Discuss.* **1979**, *67*, 286.
(12) Casavecchia, P.; Buss, R. J.; Sibener, S. J.; Lee, Y. T. *J. Chem. Phys.* **1980**, *73*, 6351.
(13) Satyapal, S.; Park, J.; Bersohn, R.; Katz, B. *J. Chem. Phys.* **1989**, *91*, 6873.
(14) Wine, P. H.; Ravishankara, A. R. *Chem. Phys.* **1982**, *69*, 365.
(15) Takahashi, K.; Wada, R.; Kawasaki, M. *J. Phys. Chem.* **1996**, *100*, 10145.
(16) Brownsword, R. A.; Hillenkamp, M.; Schmiechen, P.; Volpp, H.-R.; Upadhyaya, H. P. *J. Phys. Chem. A* **1998**, *102*, 4438.
(17) Lin, J. J.; Harich, S.; Lee, Y. T.; Yang, X. *J. Chem. Phys.* **1999**, *110*, 10821.
(18) Hack, W.; Thiesemann, H. *J. Phys. Chem.* **1995**, *99*, 17364.
(19) Wang, J.; Chen, H.; Glass, G. P.; Curl, R. F. *J. Phys. Chem. A* **2003**, *107(49)*, 10834.
(20) Pilgrim, J. S.; Jennings, R. T.; Taatjes, C. A. *Rev. Sci. Instrum.* **1997**, *68*, 1875.
(21) Selwyn, G.; Podolske, J.; Johnson, H. J. *Geophys. Res. Lett.* **1977**, *4*, 427.
(22) Zelikoff, M.; Aschenbrand, I. M. *J. Chem. Phys.* **1954**, *22*, 1685.
(23) Sun, F.; Glass, G. P.; Curl, R. F. *Chem. Phys. Lett.* **2001**, *337*, 72.
(24) Yamasaki, K.; Watanabe, A.; Kakuda, T.; Ichikawa, N.; Tokue, I. *J. Chem. Phys.* **1999**, *103*, 451.
(25) Rothman, L. S.; Barbe, A.; Benner, D. C.; Brown, L. R.; Camy-Peyret, C.; Carleer, M. R.; Chance, K.; Clerbaux, C.; Dana, V.; Devi, V. M.; Fayt, A.; Flaud, J. M.; Gamache, R. R.; Goldman, A.; Jacquemart, D.; Jucks, K. W.; Lafferty, W. J.; Mandin, J. Y.; Massie, S. T.; Nemtchinov, V.; Newnham, D. A.; Perrin, A.; Rinsland, C. P.; Schroeder, J.; Smith, K. M.; Smith, M. A. H.; Tang, K.; Toth, R. A.; Vander Auwera, J.; Varanasi, P.; Yoshino, K. *J. Quant. Spectrom., Rad. Trans.* **2003**, *82*, 5.
(26) Smith, I. W. M.; Williams, M. D. *J. Chem. Soc., Faraday II* **1985**, *81*, 1849.
(27) Abrams, M. C.; Davis, S. P.; Rao, M. L. p.; Engleman, R. *J. Mol. Spectrosc.* **1994**, *165*, 57.
(28) Papineau, N.; Flaud, J., -M.; Camy-Peyret, C.; Guelachvili, G. *J. Mol. Spectrosc.* **1981**, *87*, 219.
(29) Gierczak, T.; Talukdar, R. K.; Herndon, S.; Vaghjiani, G. L.; Ravishankara, A. R. *J. Phys. Chem. A* **1997**, *101*, 3125.
(30) Han, J.-x.; Utkin, Y. G.; Chen, H.-b.; Burns, L. A.; Curl, R. F. *J. Chem. Phys.* **2002**, *117*, 6538.
(31) Yamada, F.; Slagle, I. R.; Gutman, D. *Chem. Phys. Lett.* **1981**, *83(2)*, 409.
(32) Nesbitt, F. L.; Payne, W. A.; Stief, L. J. *J. Phys. Chem.* **1989**, *93*, 5158.
(33) Wollenhaupt, M.; Crowley, J. N. *J. Phys. Chem. A* **2000**, *104*, 6429.
(34) Chang, A. H. H.; Lin, S. H. *Chem. Phys. Lett.* **2004**, *384*, 229.
(35) Chang, A. H. H.; Lin, S. H. *Chem. Phys. Lett.* **2002**, *363(1, 2)*, 175.
(36) Albaladejo, J.; Jimenez, E.; Notario, A.; Cabanas, B.; Martinez, E. *J. Phys. Chem. A* **2002**, 106, 2512.